A Study on Underground Communication System using a Horizontal Small Antenna

Shuwei Dong, Aiguo Yao* and Fanhe Meng

Faculty of Engineering, China University of Geosciences, Wuhan 430074, Hubei, China.
* Coresonanding author: E-mail: a.yao@cug.edu.cn

Abstract - This work was about an udergground communication system which used a horizontal electrically small wire antenna to transmit electromagnetic signals from underground to ground. To solve this problem, the expressions of the magnetic vector potential and the electric field were derived. Further, a quasi-static theory was used in the condition of extremely low frequency (ELF) or super low frequency (SLF) to make an approximation on Sommerfeld integral for easy calculation. The method of moments (MOM) was applied to obtain the numerical results of the current distribution along the antenna surface. Base on the above work, the three components of the electric field versus the radial distance at different polar angles on the ground were investigated, as well as the voltage received on the ground. As a further study, the effect of the frequency and the stratum parameters on current and electric field was analyzed to acquire the characteristics of the antenna and the propagation through stratum. The results indicated that higher frequency could cause greater attenuation in the condition of ELF or SLF. The conductivity had a large influence on electric field by negative correlation while the relative permittivity had a tiny influence on electric filed by positive correlation.

Keywords - Underground communication system; Electromagnetic field; Horizontal electrically small antenna; Method of moments; Quasi-static approximation

I. INTRODUCTION

Electromagnetic underground communication plays an important role in the mine production. Through the stratum, the communication system can propagate signals from underground to ground, and the kernel technology of which is the use of underground antenna. Unlike conventional communication, the underground communication faces a series of difficulties because the transmission medium is the lossy formation, which will cause attenuation of electromagnetic waves. The issue of electromagnetic propagation through different media has been studied first by Sommerfeld [1] in 1909. Then Sommerfeld [2] established a vertical dipole model placed at the surface of ground and used the evaluation of Fourier-Bessel integrals to solve it. Moore and Blair [3] gave the field expressions of a dipole near a conducting half space in 1961. Bannister [4-6] studied the quasi-static field of antennas using complex image theory for many years, and in 1979 he wrote an article to summarize his work. Chang and Wait [7] did the study of a horizontal wire antenna which located above or buried in the ground with extremely low frequency, and derived the expressions of propagation constant in 1974. In 1990, King [8] did the study about a dipole above an imperfectly conducting half space. In 1997, King, Harrison and Houdzoumis [9] gave the results of electromagnetic fields of a very low frequency antenna in the sea. Tai [10] studied the radiation of a dipole immersed in a dissipative medium in 2000. In 2004, Thottappillil, Uman and Theethayi [11] gave the expressions of a semi infinite antenna above a conducting plane. Vong, Rodger and Marshall [12] modeled an electromagnetic telemetry system and gave a portion of results in 2005. Xu and Huang [13] used an efficient computation to solve the problem of an electric dipole above a lossy half-space in 2007. Khalatpour, Sarraf Shirazi and Moradi [14] used numerical methods to study a wire antenna above a lossy half space in 2010. Parise [15] did a research on quasi-static theory and obtained the harmonic electromagnetic feld components excited by a vertical electric dipole lying on the surface of a flat and homogeneous lossy half-space in 2013. In addition, there are many scholars who have done researches on related problems. However, the detailed study of a horizontal electrically small antenna in a lossy medium has been not common in previous researches. A horizontal electrically small antenna with ELF or SLF is the best choice for underground electromagnetic communication generator, which can be used effectively in mine communication. This kind of antenna can play a good role in other areas such as energy development, trenchless technology, measurement while drilling, geophysical prospecting, lateral wells butt and monitoring of underground targets as well.

In this paper, an accurate model about a horizontal electrically small antenna located underground with ELF or SLF has been proposed. Analytical solutions of the field excited by underground antenna have been obtained to solve this problem. Sommerfeld integral in the expressions can cause some troubles on calculation, so quasi-static approximation has been used to solve the problems in this

low frequency problem. The main work is to get the induction field of the electrically small antenna, for this purpose, numerical methods including the MOM have been used. Numerical results such as the current distribution and the electric field have been obtained in order to describe the antenna character. As a further study, the effect of outside parameters on induction field has been considered and the variation curves of the current and the electric field with the frequency or the stratum parameters have been got for better understanding of the antenna.

II. MATHEMATICAL MODEL

Treat earth as a homogenous medium, the magnetic vector potential $\mathbf{A}$ satisfies the equation (1) obtained from the Maxwell's equations.

$$\nabla^2\mathbf{A}+k^2\mathbf{A}=-\mu\mathbf{J} \tag{1}$$

where $\mathbf{J}$ is the current density of an impressed source, k is the wave number given by $k^2=-i\omega\mu(\sigma+i\omega\varepsilon)$, and ε, μ and σ are, respectively, the permittivity, permeability and conductivity of the medium, ω is the angular frequency. What should be noted is that the time dependence $e^{i\omega t}$ is assumed and suppressed in this equation and the following analysis.

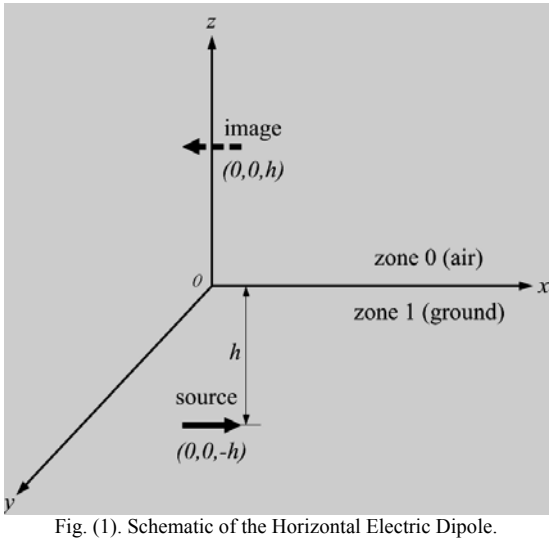

Fig. (1). Schematic of the Horizontal Electric Dipole.

As shown in Fig. 1, the air occupies the upper half space referred as medium 0 whereas the ground occupies the lower one referred as medium 1, and the coordinate origin is at the interface. The horizontal electric dipole is oriented in the x direction and located at the coordinates $(0,0,-h)$, while the coordinates of its image are $(0,0,h)$, where $h>0$. Considering that the dipole is represented by the current density $\mathbf{J}=Il\delta(\mathbf{r}-\mathbf{r}')\mathbf{e}_x$, The magnetic vector potentials in two media satisfies with the following two equations (2) and (3), respectively.

$$\nabla^2\mathbf{A}_0+{k_0}^2\mathbf{A}_0=0 \tag{2}$$

$$\nabla^2\mathbf{A}_1+{k_1}^2\mathbf{A}_1=-\mu Il\delta(\mathbf{r}-\mathbf{r}')\mathbf{e}_x \tag{3}$$

From the boundary conditions, there are two components of the magnetic vector potential oriented x and z direction respectively. The field generated by the horizontal dipole is the superposition of the primary field and the reflected field of the source, which can be derived by the image theory. According to what we have known of the magnetic vector potentials in free-space, the x component of the vector potentials in two media satisfies the equations (4) and (5).

$$A_{0x}=\frac{\mu Il}{4\pi}\int_0^\infty P\frac{k_\rho}{\xi_0}e^{-\xi_0|z+h|}J_0(k_\rho\rho)dk_\rho \tag{4}$$

$$A_{1x}=\frac{\mu Il}{4\pi}\int_0^\infty\left(\frac{k_\rho}{\xi_1}e^{-\xi_1|z+h|}+Q\frac{k_\rho}{\xi_1}e^{-\xi_1|z-h|}\right)J_0(k_\rho\rho)dk_\rho \tag{5}$$

where P and Q are undetermined coefficients determined by the boundary conditions, and J_0 is the zero-order Bessel function of the first kind. Here some variables are given by $\rho^2=x^2+y^2$, ${k_\rho}^2={k_x}^2+{k_y}^2$, ${\xi_0}^2={k_\rho}^2-{k_0}^2$ and ${\xi_1}^2={k_\rho}^2-{k_1}^2$, where k_0 and k_1 are, respectively, the wave numbers of the air and the ground.

The boundary conditions are given by the equations (6) and (7), from which the relationship equations between P and Q can be derived.

$$\lim_{z\to0+}A_{0x}=\lim_{z\to0-}A_{1x} \tag{6}$$

$$\lim_{z\to0+}\frac{\partial A_{0x}}{\partial z}=\lim_{z\to0-}\frac{\partial A_{1x}}{\partial z} \tag{7}$$

Further, the coefficients P and Q are obtained as the expressions (8) and (9).

$$P=\frac{2\xi_0}{\xi_1+\xi_0}e^{(\xi_0-\xi_1)h} \tag{8}$$

$$Q=\frac{2\xi_1}{\xi_1+\xi_0}-1 \tag{9}$$

So far, the x component of the vector potentials in two media can be expressed as the following expressions (10) and (11).

$$A_{0x}=\frac{\mu Il}{4\pi}I_{0x} \tag{10}$$

$$A_{1x}=\frac{\mu Il}{4\pi}\left(\frac{e^{-ik_1R}}{R}-\frac{e^{-ik_1R_i}}{R_i}+I_{1x}\right) \tag{11}$$

$$I_{0x}=\int_0^\infty\frac{2k_\rho}{\xi_1+\xi_0}e^{-\xi_0z-\xi_1h}J_0(k_\rho\rho)dk_\rho \tag{12}$$

$$I_{1x}=\int_0^\infty\frac{2k_\rho}{\xi_1+\xi_0}e^{-\xi_0z-\xi_1h}J_0(k_\rho\rho)dk_\rho \tag{13}$$

where $R=\sqrt{\rho^2+(z+h)^2}$ and $R_i=\sqrt{\rho^2+(z-h)^2}$.

The following work is to solve the z component of the vector potentials. Since it is independent of the source, the wave equations (14) and (15) can be got.

$$\nabla^2 A_{0z} + {k_0}^2 A_{0z} = 0 \tag{14}$$

$$\nabla^2 A_{1z} + {k_1}^2 A_{1z} = 0 \tag{15}$$

According to the knowledge of partial differential equations, the general solutions of (14) and (15) in a cylindrical coordinate system (ρ,θ,z) are as follows.

$$A_{0z} = \frac{\mu I l}{4\pi}\sum_{n=-\infty}^{\infty} \mathrm{e}^{in\theta}\int_0^{\infty}\left(a_{0n}\mathrm{e}^{-\xi_0 z} + b_{0n}\mathrm{e}^{\xi_0 z}\right)J_n\left(k_\rho\rho\right)\mathrm{d}k_\rho \tag{16}$$

$$A_{1z} = \frac{\mu I l}{4\pi}\sum_{n=-\infty}^{\infty} \mathrm{e}^{in\theta}\int_0^{\infty}\left(a_{1n}\mathrm{e}^{-\xi_1 z} + b_{1n}\mathrm{e}^{\xi_1 z}\right)J_n\left(k_\rho\rho\right)\mathrm{d}k_\rho \tag{17}$$

Because of $\lim_{z\to\infty}\mathrm{e}^{\xi_0 z} = 0$ and $\lim_{z\to-\infty}\mathrm{e}^{-\xi_1 z} = 0$, in order to ensure A_{0z} and A_{1z} are finite, the coefficients b_{0n} and a_{1n} must be 0. Meanwhile, the vector potential satisfies $A_{0z}(\rho,\theta,z) = A_{0z}(\rho,-\theta,z)$ and $A_{1z}(\rho,\theta,z) = A_{1z}(\rho,-\theta,z)$, so A_{0z} and A_{1z} are expressed by (18) and (19).

$$A_{0z} = \frac{\mu I l}{4\pi}\sum_{n=-\infty}^{\infty} \cos\theta\int_0^{\infty} a_n\mathrm{e}^{-\xi_0 z}J_n\left(k_\rho\rho\right)\mathrm{d}k_\rho \tag{18}$$

$$A_{1z} = \frac{\mu I l}{4\pi}\sum_{n=-\infty}^{\infty} \cos\theta\int_0^{\infty} b_n\mathrm{e}^{\xi_1 z}J_n\left(k_\rho\rho\right)\mathrm{d}k_\rho \tag{19}$$

The boundary conditions related to A_{0z} and A_{1z} are as follows.

$$\lim_{z\to 0+} A_{0z} = \lim_{z\to 0-} A_{1z} \tag{20}$$

$$\lim_{z\to 0+}\frac{1}{{k_0}^2}\left(\frac{\partial A_{0x}}{\partial x} + \frac{\partial A_{0z}}{\partial z}\right) = \lim_{z\to 0-}\frac{1}{{k_1}^2}\left(\frac{\partial A_{1x}}{\partial x} + \frac{\partial A_{1z}}{\partial z}\right) \tag{21}$$

By using the boundary conditions, the z component of the vector potentials in two media are got respectively.

$$A_{0z} = \frac{\mu I l\cos\theta}{4\pi} I_{0z} \tag{22}$$

$$A_{1z} = \frac{\mu I l\cos\theta}{4\pi} I_{1z} \tag{23}$$

$$I_{0z} = \int_0^{\infty}\frac{2\left({k_0}^2 - {k_1}^2\right){k_\rho}^2}{\left(\xi_1+\xi_0\right)\left({k_0}^2\xi_1 + {k_1}^2\xi_0\right)}\mathrm{e}^{-\xi_1 h - \xi_0 z}J_1\left(k_\rho\rho\right)\mathrm{d}k_\rho \tag{24}$$

$$I_{1z} = \int_0^{\infty}\frac{2\left({k_0}^2 - {k_1}^2\right){k_\rho}^2}{\left(\xi_1+\xi_0\right)\left({k_0}^2\xi_1 + {k_1}^2\xi_0\right)}\mathrm{e}^{\xi_1(z-h)}J_1\left(k_\rho\rho\right)\mathrm{d}k_\rho \tag{25}$$

The magnetic vector potential underground is obtained so far, and it is

$$\mathbf{A}_1 = \frac{\mu I l}{4\pi}\left[\left(\frac{\mathrm{e}^{-ik_1R}}{R} - \frac{\mathrm{e}^{-ik_1R_i}}{R_i} + I_{1x}\right)\mathbf{e}_x + \cos\theta I_{1z}\mathbf{e}_z\right] \tag{26}$$

In the following analysis, what we are concerned is the vector potential underground presented as $\mathbf{A}_1$. For simplicity, the subscript 1 will be omitted. From Maxwell's equations, the relationship expression between the electric field $\mathbf{E}$ and the vector potential $\mathbf{A}$ is shown as

$$\mathbf{E} = -i\omega\mathbf{A} + \frac{1}{\mu\sigma + i\omega\mu\varepsilon}\nabla\nabla\bullet\mathbf{A} \tag{27}$$

To solve the electric field $\mathbf{E}$, $\nabla\bullet\mathbf{A}$ should be solved first. Since $A_\rho = \cos\theta A_x$ and $A_\theta = -\sin\theta A_x$, the expression of $\nabla\bullet\mathbf{A}$ can be derived in cylindrical coordinate system (ρ,θ,z).

$$\nabla\bullet\mathbf{A} = \frac{1}{\rho}\frac{\partial\left(\rho A_\rho\right)}{\partial\rho} + \frac{1}{\rho}\frac{\partial A_\theta}{\partial\theta} + \frac{\partial A_z}{\partial z} = \frac{\partial A_\rho}{\partial\rho} + \frac{\partial A_z}{\partial z} \tag{28}$$

By using the recurrence formula $\partial J_0\left(k_\rho\rho\right)/\partial\rho = -k_\rho J_1\left(k_\rho\rho\right)$, the following result is acquired.

$$\frac{\partial A_z}{\partial z} = -\frac{\mu I l\cos\theta}{4\pi}\frac{\partial}{\partial\rho}I_{1z'} \tag{29}$$

$$I_{1z'} = \int_0^{\infty}\frac{2\left({k_0}^2 - {k_1}^2\right)k_\rho\xi_1}{\left(\xi_1+\xi_0\right)\left({k_0}^2\xi_1 + {k_1}^2\xi_0\right)}\mathrm{e}^{\xi_1(z-h)}J_0\left(k_\rho\rho\right)\mathrm{d}k_\rho \tag{30}$$

Then

$$\nabla\bullet\mathbf{A} = \frac{\mu I l}{4\pi}\cos\theta\frac{\partial}{\partial\rho}\left(\frac{\mathrm{e}^{-ik_1R}}{R} - \frac{\mathrm{e}^{-ik_1R_i}}{R_i} + I_A\right) \tag{31}$$

$$I_A = \int_0^{\infty}\frac{2{k_1}^2 k_\rho}{{k_0}^2\xi_1 + {k_1}^2\xi_0}\mathrm{e}^{\xi_1(z-h)}J_0\left(k_\rho\rho\right)\mathrm{d}k_\rho \tag{32}$$

Therefore, the three components of the electric field can be obtained.

$$E_\rho = \frac{\cos\theta I l}{4\pi\left(\sigma_1 + i\omega\varepsilon_1\right)}\left[\begin{array}{l}{k_1}^2\left(\dfrac{\mathrm{e}^{-ik_1R}}{R} - \dfrac{\mathrm{e}^{-ik_1R_i}}{R_i} + I_{1x}\right)\\ +\dfrac{\partial^2}{\partial\rho^2}\left(\dfrac{\mathrm{e}^{-ik_1R}}{R} - \dfrac{\mathrm{e}^{-ik_1R_i}}{R_i} + I_A\right)\end{array}\right] \tag{33}$$

$$E_\theta = -\frac{\sin\theta I l}{4\pi\left(\sigma_1 + i\omega\varepsilon_1\right)}\left[\begin{array}{l}{k_1}^2\left(\dfrac{\mathrm{e}^{-ik_1R}}{R} - \dfrac{\mathrm{e}^{-ik_1R_i}}{R_i} + I_{1x}\right)\\ +\dfrac{1}{\rho}\dfrac{\partial}{\partial\rho}\left(\dfrac{\mathrm{e}^{-ik_1R}}{R} - \dfrac{\mathrm{e}^{-ik_1R_i}}{R_i} + I_A\right)\end{array}\right] \tag{34}$$

$$E_z = \frac{\cos\theta I l}{4\pi\left(\sigma_1 + i\omega\varepsilon_1\right)}\frac{\partial^2}{\partial z\partial\rho}\left(\frac{\mathrm{e}^{-ik_1R}}{R} + \frac{\mathrm{e}^{-ik_1R_i}}{R_i} - \frac{{k_0}^2}{{k_1}^2}I_A\right) \tag{35}$$

One existed problem is how to solve the Sommerfeld integrals in the field expressions. Under the condition of ELF or SLF, the field is in quasi-static situation. In order to facilitate the calculation, the quasi-static approximations can be used. In this case, Wait [16] have shown that ${k_0}^2\xi_1 + {k_1}^2\xi_0 \approx {k_1}^2\xi_0$, $\xi_0 = \sqrt{{k_\rho}^2 - {k_0}^2} \approx k_\rho$, and these approximations have verified available by many scholars, such as Cooray [17]. In addition, a Wait and Spies [18] image theory approximation is utilized here.

$$\frac{\xi_1 - k_\rho}{\xi_1 + k_\rho} \approx \mathrm{e}^{-k_\rho d} \tag{36}$$

where $d = \delta(1-i)$, and δ is the skin depth given by $\delta = \sqrt{1/\pi f \mu \sigma_1}$.

Thus, by using the quasi-static approximations, it is possible to obtain the approximate expressions of Sommerfeld integrals I_{1x} and I_A as follows.

$$\begin{aligned} I_{1x} &= \int_0^\infty \frac{2k_\rho}{\xi_1 + k_\rho} \mathrm{e}^{\xi_1(z-h)} J_0(k_\rho \rho) \mathrm{d}k_\rho \\ &\approx \int_0^\infty \left(1 - \mathrm{e}^{-k_\rho d}\right) \mathrm{e}^{\xi_1(z-h)} J_0(k_\rho \rho) \mathrm{d}k_\rho = A - B \end{aligned} \tag{37}$$

$$A = \int_0^\infty \mathrm{e}^{\xi_1(z-h)} J_0(k_\rho \rho) \mathrm{d}k_\rho \tag{38}$$

$$B = \int_0^\infty \mathrm{e}^{-k_\rho d} \mathrm{e}^{\xi_1(z-h)} J_0(k_\rho \rho) \mathrm{d}k_\rho \tag{39}$$

$$I_A \approx 2\int_0^\infty \mathrm{e}^{\xi_1(z-h)} J_0(k_\rho \rho) \mathrm{d}k_\rho \tag{40}$$

Use the approximation that Bannister and Dube [5] have verified as $\mathrm{e}^{\xi_1(z-h)} \approx \mathrm{e}^{ik_1 m(z-h)} \mathrm{e}^{k_\rho n(z-h)}$, where the constants m and n get values variable for different cases. When $\sqrt{\rho^2 + (z-h)^2} << \delta$ (δ is the skin depth), $m = 0$ and $n = 1$. When $\sqrt{\rho^2 + (z-h)^2}$ and δ are of the same order of magnitude, with $m = 0.4$ and $n = 0.96$ for $\sqrt{\rho^2 + (z-h)^2} / \delta < 1$ while $m = 0.96$ and $n = 0.4$ for $1 < \sqrt{\rho^2 + (z-h)^2} / \delta < 10$. This approximation has a good match presented in the paper written by Gavriloska, Mircev and Arnautovski, et al [19].

Utilizing the Sommerfeld identity [20]

$$\int_0^\infty \frac{\mathrm{e}^{-\xi(z-h)}}{\xi} J_0(k_\rho \rho) k_\rho \mathrm{d}k_\rho = \frac{\mathrm{e}^{-ikR}}{R} \tag{41}$$

Then

$$\begin{aligned} A &\approx \mathrm{e}^{ik_1 m(z-h)} \int_0^\infty \mathrm{e}^{k_\rho n(z-h)} J_0(k_\rho \rho) \mathrm{d}k_\rho \\ &= \frac{\mathrm{e}^{-ik_1 m(-z+h)}}{\sqrt{\rho^2 + [n(-z+h)]^2}} \end{aligned} \tag{42}$$

$$\begin{aligned} B &\approx \int_0^\infty \mathrm{e}^{-k_\rho d} \mathrm{e}^{ik_1 m(z-h)} \mathrm{e}^{k_\rho n(z-h)} J_0(k_\rho \rho) \mathrm{d}k_\rho \\ &= \frac{\mathrm{e}^{-ik_1 m(-z+h)}}{\sqrt{\rho^2 + [n(-z+h) + d]^2}} \end{aligned} \tag{43}$$

$$\begin{aligned} I_A &\approx 2\mathrm{e}^{ik_1 m(z-h)} \int_0^\infty \mathrm{e}^{k_\rho n(z-h)} J_0(k_\rho \rho) \mathrm{d}k_\rho \\ &= \frac{2\mathrm{e}^{-ik_1 m(-z+h)}}{\sqrt{\rho^2 + [n(-z+h)]^2}} \end{aligned} \tag{44}$$

Thus, the three components of the electric field can be defined by more easily calculated expressions, thereby eliminating the difficulties in computing the Sommerfeld integrals. To obtain the electric field, which should be done first is to calculate the current distribution along the antenna. Taking the field point coordinates and the source point coordinates are, respectively, (x, y, z) and (x', y', z'). The horizontal antenna is oriented along x axial, and the coordinates of its center point are $(0, 0, z')$. Considering the current distributes on the antenna surface only, the x component of the electric field generated by current is $\mathbf{E}_x$ while the x component of the electric field generated by other sources is $\mathbf{E}^i{}_x$. Because the antenna surface is considered to be an ideal conductor, according to the boundary conditions of the ideal conductor, the following equation (45) should be satisfied.

$$\mathbf{E}_x(\mathbf{s}) + \mathbf{E}^i{}_x(\mathbf{s}) = 0 \tag{45}$$

Since the antenna radius a and the wavelength λ meet the condition $a << \lambda$, the assumption that current is uniformly distributed along the surface is defined. Then the effect of the current along the antenna surface is equivalent to a line current along x axis.

The MOM [21] is used to obtain the current distribution, and in this case the MOM formula of the horizontal antenna is as shown in (46). In order to get the numerical result, pulse base and point matching method are used in this section.

$$\begin{aligned} E^i{}_x &= -\frac{Il}{4\pi(\sigma_1 + i\omega\varepsilon_1)} \times \\ &\int_l I(x') \left[\begin{aligned} &k_1{}^2 \left(\frac{\mathrm{e}^{-ik_1 R}}{R} - \frac{\mathrm{e}^{-ik_1 R_i}}{R_i} + I_{1x} \right) \\ &+ \frac{\partial^2}{\partial x^2} \left(\frac{\mathrm{e}^{-ik_1 R}}{R} - \frac{\mathrm{e}^{-ik_1 R_i}}{R_i} + I_A \right) \end{aligned} \right] \mathrm{d}x' \end{aligned} \tag{46}$$

where $R = \sqrt{a^2 + (x - x')^2}$ and $R_i = \sqrt{a^2 + (x + x')^2}$.

Based on the above work, the three components of the electric field are easily computed by utilizing the formulas (33-35). Finally, the voltage received by the wire antenna on the ground should be obtained as a parameter can be directly measured on the ground. Formula (47) shows the expression of the voltage received on the ground by making use of E_ρ .

$$V_r = \sum_i^N \frac{E_\rho(\rho_i) + E_\rho(\rho_{i+1})}{2} (\rho_{i+1} - \rho_i) \tag{47}$$

where V_r is the voltage received on the ground, and ρ_i is the distance of the i th point.

III. NUMERICAL RESULTS AND DISCUSSION

A. Field of the Antenna

Consider an underground horizontal wire antenna which is located 500 m down from the ground surface as the signal generator. The ground is seen as a homogenous medium, and the characters are $\sigma = 0.075$ S/m, $\varepsilon = 20\varepsilon_0 = 1.7708\times10^{-10}$ F/m and $\mu = 4\pi\times10^{-7}$ H/m. The length of the antenna is $l = 6$ m while the radius is $a = 0.05$ m. As the feed terminal, there is a 1 V δ voltage source excitation added on the center, where the δ gap is 0.1 m. In the following work, we take the modulus of the complex numbers as the values of the current.

The current distribution of the horizontal antenna is calculated by MOM, Fig. 2 shows the current distribution on the wire antenna surface when the frequency is 10 Hz. The current distribution is approximate triangular distribution, which well matches the known current distribution of electrically small antenna.

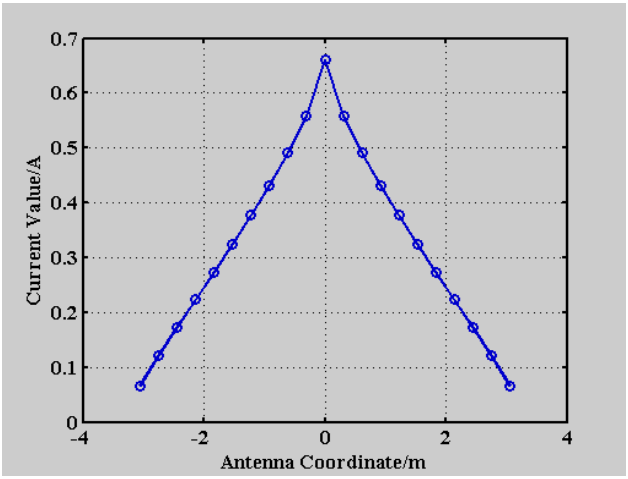

Fig. (2). Current Distribution on the Wire Antenna Surface.

The electric field on the ground plane is obtained afterwards. The magnitude and the phase of the field are both analyzed to know the field more clearly. Fig. 3 shows the curves of the three components of the electric field magnitude along the radial distance while Fig. 4 shows the curves of the magnitude at different radial distances with the polar angle in polar coordinates.

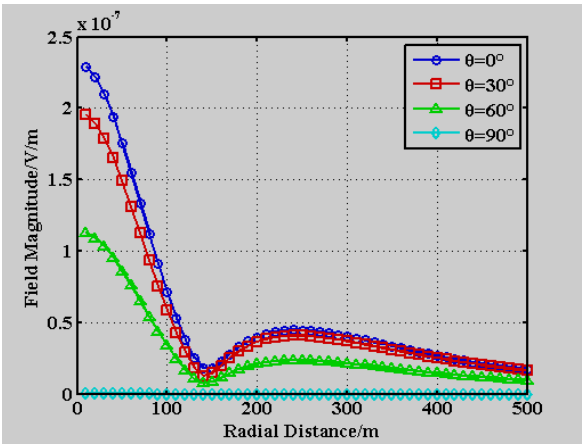

(a)

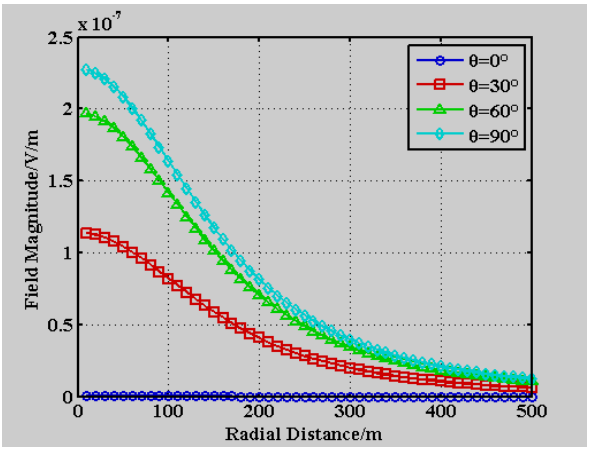

(b)

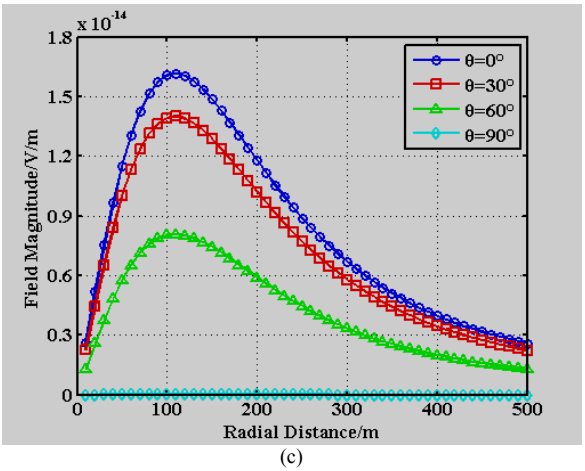

(c)

Fig. (3). Curves of (a) the Radial Component, (b) the Tangential Component and (c) the Axial Component of the Electric Field Magnitude with the Radial Distance.

The curves in Fig. 3 (a) represent the variation of the radial component of the electric field along the radial distance in different polar angles. The magnitude of the radial component of the electric field goes through a

process that gets smaller to a minimum value from the maximum value first and then gets bigger and afterwards gets smaller gently again along the radial distance in all polar angles. When the polar angel $\theta = 0°$, the magnitude is larger than the corresponding ones in the same radial distance when the polar angle takes other values. Curves on Fig. 3 (b) show the variation of the tangential component of the electric field, from which we can see the magnitude gets smaller with the increasing radial distance, and the magnitude reaches maximum when the polar angel $\theta = 90°$. The axial component of the electric field magnitude becomes larger with the increasing distance first, and then becomes smaller when after a maximum value, which is shown in Fig. 3 (c). The trends of the axial component of the electric field with the radial distance at different polar angles are the same, but the value at $\theta = 0°$ is larger than the others. Compared with the other two components, the axial component of the electric field is several orders of magnitude smaller. The curves of the electric field magnitude with the polar angle are shown in Fig. 4, they are symmetrical in the polar coordinates and shaped almost like circles in corresponding half areas.

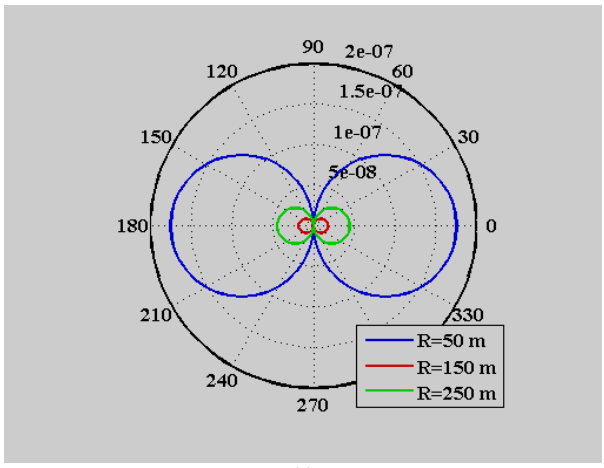

(a)

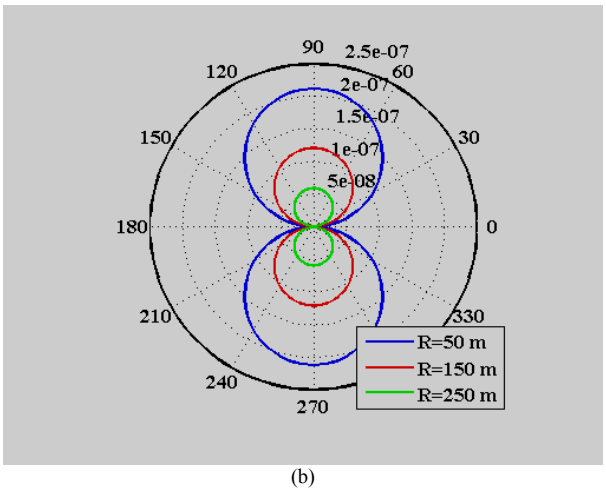

(b)

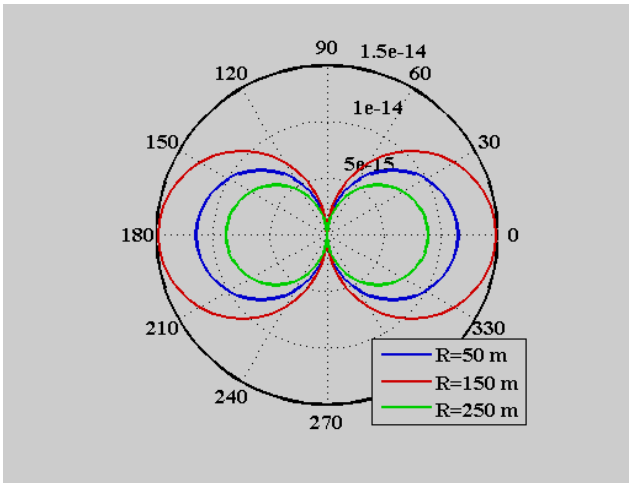

(c)

Fig. (4). Curves of (a) the Radial Component, (b) the Tangential Component and (c) the Axial Component of the Electric Field Magnitude with the Polar Angle.

The phase of the electric field is also studied as shown in Fig. 5. The phase of the radial component of the electric field undergoes a mutation at the radial distance between 150-200 m, and the other two components get gradually increase with the increasing radial distance. The phase mutation point is exactly the minimum point of the magnitude, which illustrates the direction of the radial component of the electric field changes in this point. In addition, the trends of the phase variation with the radial distance at different polar angles are similar.

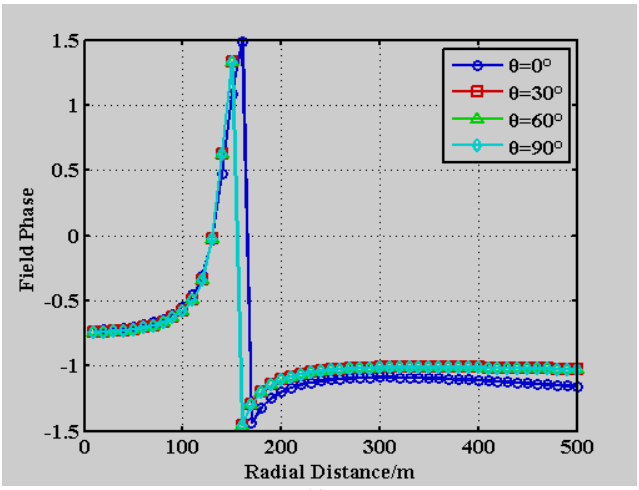

(a)

Fig. (5). Curves of (a) the Radial Component, continues on next page.

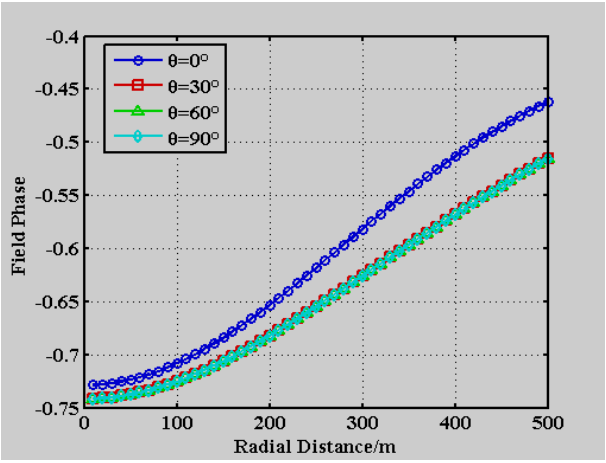

(b)

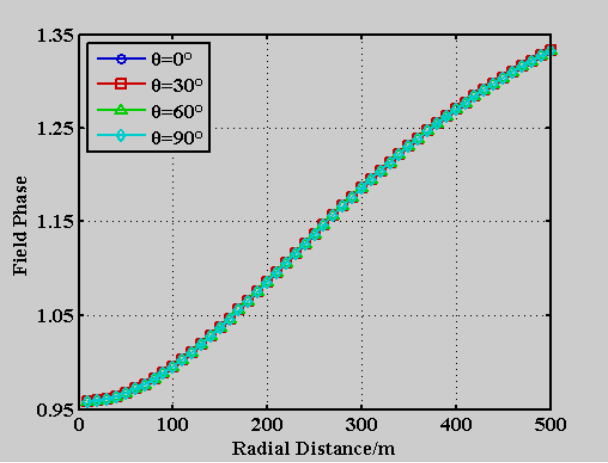

(c)

Fig. (5). Curves of (a) the Radial Component, (b) the Tangential Component and (c) the Axial Component of the Electric Field Phase with the Radial Distance.

Fig. 6 shows the curves about the variation of the total electric field with the radial distance on the ground. The curve generally presents a tendency which the field magnitude decreases with the increasing distance.

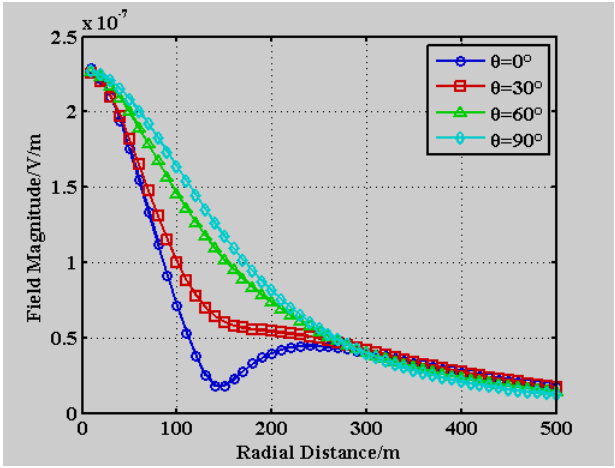

Fig. (6). Curves of the Total Electric Field Magnitude with the Radial Distance.

The curve of the voltage received on the ground with the radial distance is shown in Fig. 7. Here the original point on the ground is taken as the relative voltage zero point, and the voltage value is gained at the polar angle $\theta = 0°$. The received voltage value tends to increase first, and gets to decrease after a maximum value. The maximum value appears at the point that the direction of the radial component of the electric field begins to change.

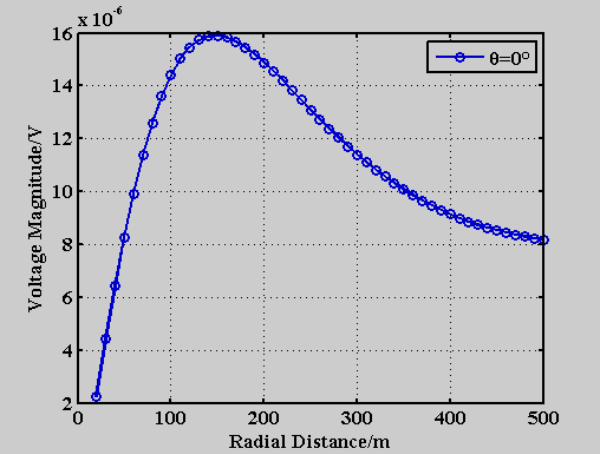

Fig. (7). Curve of the Voltage Received on the Ground with the Radial Distance.

B. Influence of the Frequency on Field

In lossy medium, the attenuation of the electric field increases as the frequency gets higher, so the frequency is an important parameter that can influence the electric field on the ground. The maximum value of the current on the antenna surface is chosen to study the influence of the frequency on current distribution. In Fig. 8, it is shown that the current value tends to decrease with the increasing frequency, but the influence is too tiny to distinguish the size of the value.

In this case, the radial component of the electric field is of our most concern, which directly affects the voltage received, so the radial component of the electric field can be a representative to study the influence on electric field. Three points corresponding to the radial distance $R = 50$ m, $R = 150$ m and $R = 250$ m at the polar angle $\theta = 0°$ are taken as the study objects. As shown in Fig. 9, the field value at the points whose radial distance $R = 50$ m and $R = 250$ m decreases when the frequency increases, but the field value at the point $R = 150$ m gets a slight increase when the frequency increases. The point $R = 150$ m is just in the vicinity of the point where the radial component of the electric field magnitude takes the minimum value and the field phase undergoes a mutation. This shows that the radial distance of the mutation point increases with the increasing frequency.

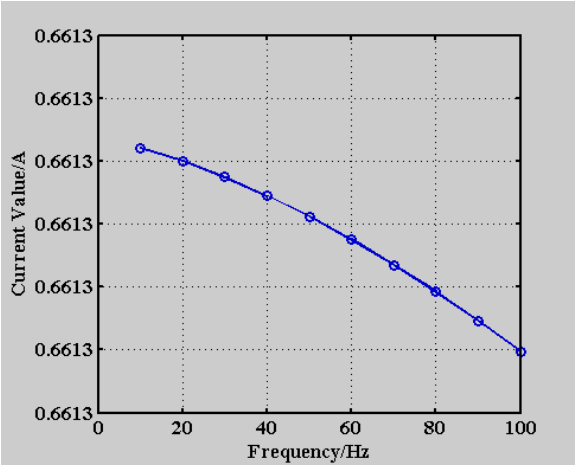

Fig. (8). Curve of the Maximum Current Value with the Frequency.

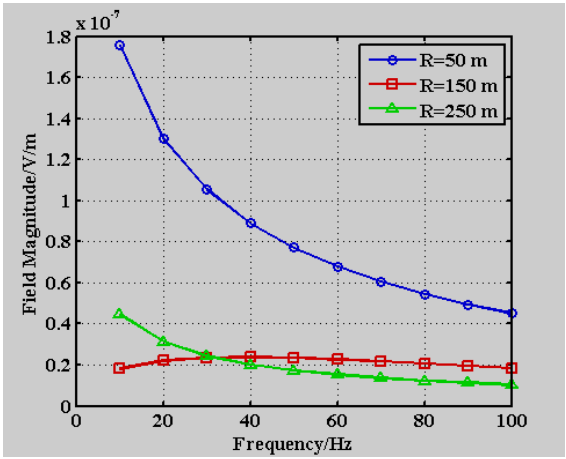

Fig. (9). Curves of the Radial Component of the Electric field Magnitude with the Frequency.

C. Influence of the Stratum Parameters on Field

The characteristic of the formation affects the field as well, two of which are the stratum conductivity and the relative permittivity. Similar with the previous study on frequency, we choose the maximum current value on antenna surface as the object to study the influence on current, and use the radial component of the electric field magnitude corresponding to the points $R = 50$ m, $R = 150$ m and $R = 250$ m at the polar angle $\theta = 0°$ to study the influence on electric field. Fig. 10 shows the curve of current value varying with the conductivity, which indicates that the current value has a positive correlation with the conductivity. Curves in Fig. 11 demonstrate the variation of the radial component of the electric field magnitude with the conductivity from 0.05-0.1 S/m at the three points selected. With the increasing conductivity, the field magnitudes at the three points all get smaller. There are obvious variation at the points $R = 50$ m and $R = 250$ m while unconspicuous variation at the point $R = 150$ m.

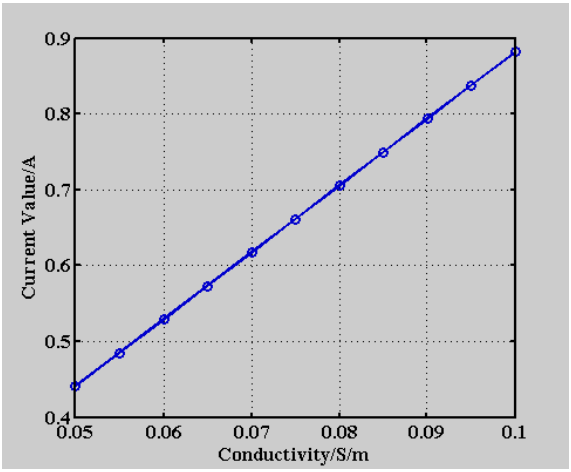

Fig. (10). Curve of the Maximum Current Value with the Conductivity.

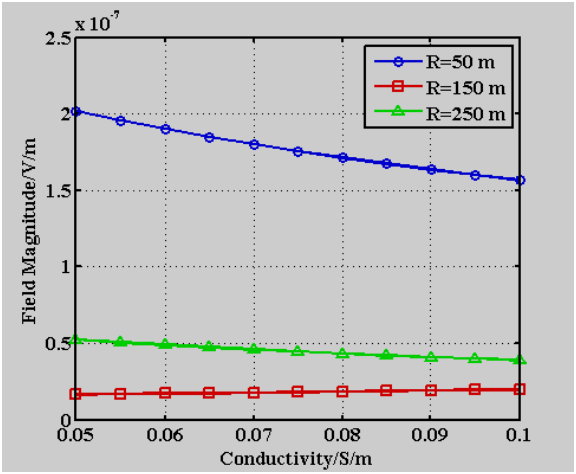

Fig. (11). Curves of the Radial Component of the Electric Field Magnitude with the Conductivity.

The effect of the relative permittivity on current and electric field is studied later. Curve on Fig. 12 represents the variation of the current value on antenna surface with

the relative permittivity. The current value increases when the relative permittivity gets larger, but the influence is so tiny that the change is not obvious. Fig. 13 represents the dependence of the radial component of the electric field with the relative permittivity corresponding to the point $R = 50$ m at the angle $\theta = 0°$. The value of the radial component of the electric field is positively correlated with the relative permittivity, and the variation is too micro to recognize the difference of the value as well.

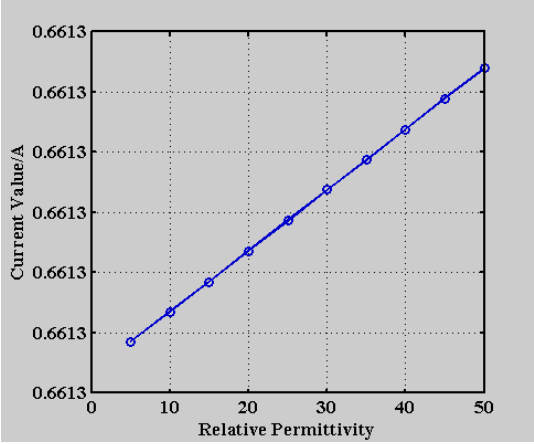

Fig. (12). Curve of the Maximum Current Value with the Relative Permittivity.

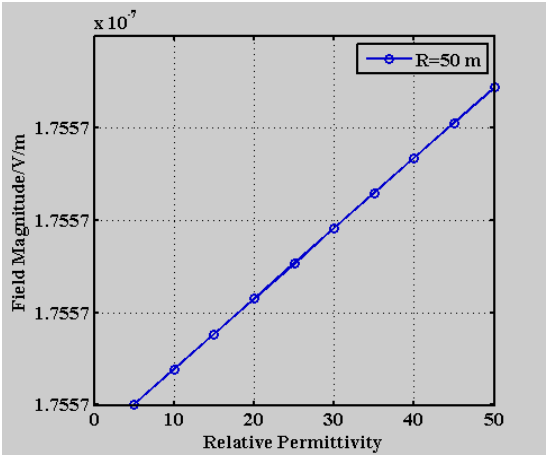

Fig. (13). Curve of the Radial Component of the Electric Field Magnitude with the Relative Permittivity.

D. Verification

In order to verify the numerical results, a simulation model by using the commercial software HFSS was done. The model simulated is the same as the previous study with 10 Hz frequency. The ground characters are $\sigma = 0.075$ S/m, $\varepsilon = 20\varepsilon_0 = 1.7708 \times 10^{-10}$ F/m and $\mu = 4\pi \times 10^{-7}$ H/m. The current distribution on antenna surface is presented in Fig. 14, which matches well with the previous result in Fig. 2. Curve on Fig. 15 shows the variation of the total field along the radial distance. The electric field value in this case is a little smaller than the result in Fig. 6. This consequence may due to that more factors are concerned in HFSS and the model in this work is too large to calculate. Overall, this HFSS case is largely consistent with the previous results as verification.

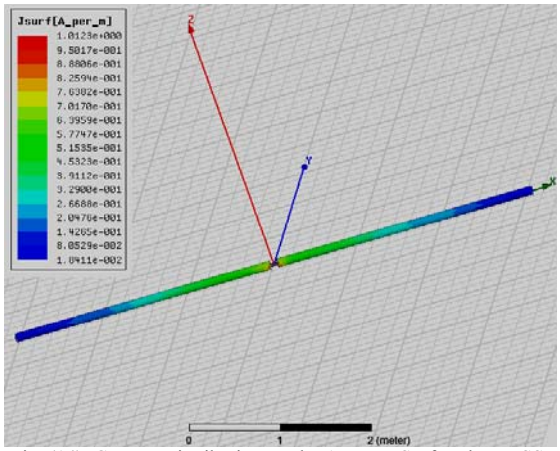

Fig. (14). Current Distribution on the Antenna Surface by HFSS.

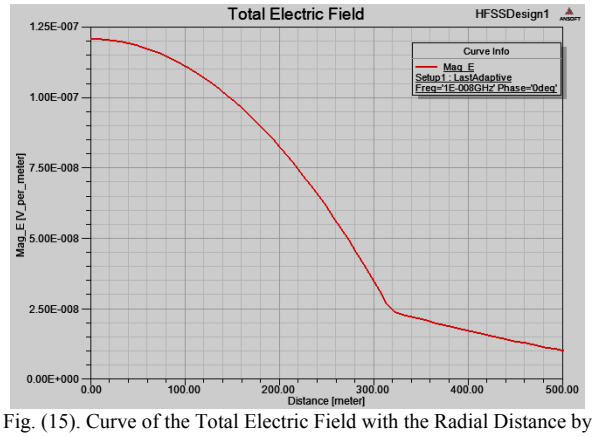

Fig. (15). Curve of the Total Electric Field with the Radial Distance by HFSS.

IV. CONCLUSION

In this work, a more accurate model of horizontal electrically small antenna was established to solve the problem of through the earth communication. The expressions of the electric field generated by an underground horizontal electrically small antenna were derived in forms can be easily solved in this mathematical model. Based on these work, numerical method was used to obtain the current distribution on antenna surface and the electric field on the ground in the condition of 10 Hz. In these results, the variations of three components of the electric field versus the radial distance at different polar angles were investigated respectively. The radial and axial components of the electric field got the maximum value at the polar angle $\theta = 0°$, and the tangential component of the

electric field got the maximum value at the polar angle $\theta = 90°$. With the increasing radial distance, the radial component of the electric field at the polar angle $\theta = 0°$ decreased first, and achieved the minimum value at the phase mutation point $R = 150$ m, then made a change of getting larger and afterwards smaller again. The tangential component of the electric field at the polar angle $\theta = 90°$ diminished with the radial distance, and the axial component of the electric field at the polar angle $\theta = 0°$ appeared a trend that increased first and decreased afterwards with the increasing radial distance. In addition, the voltage received on the ground was obtained. At the polar angle $\theta = 0°$, the maximum value of the voltage received was approximately at the radial distance $R = 150$ m. From the received voltage signal, we could get the information transferred from underground.

In order to have a relatively overall understanding of the antenna, the study on field variation versus the frequency was done. The consequence showed that higher frequency would cause greater attenuation on the radial component of the electric field. The influence of the stratum parameters including conductivity and relative permittivity on field was studied to make us know the propagation characteristics of the antenna through formation more clearly. The conductivity had a great impact on current and electric field, and the radial component of the electric field concerned got smaller when the conductivity got larger. The relative permittivity had a tiny impact on current and electric field, and there was a positive correlation between the radial component of the electric field and the relative permittivity.

CONFLICT OF INTEREST

The authors confirm that this article content has no conflicts of interest.

ACKNOWLEDGMENT

This work is supported by the China Geological Survey Program (No. KZ11Z245).

REFERENCES

[1] A. Sommerfeld, “Über die ausbreitung der wellen in der drahtlosen telegraphie,” Annalen der Physik, vol. 333, no. 4, pp. 665-736, 1909.

[2] A. Sommerfeld, “Über die ausbreitung der wellen in der drahtlosen telegraphie,” Annalen der Physik, vol. 386, no. 25, pp. 1135-1153, 1926.

[3] R. Moore and W. Blair, “Dipole radiation in a conducting half-space,” Journal of Research of the National Bureau of Standards-D. Radio Propagation, vol. 65, no. 6, pp. 547-563, 1961.

[4] P. R. Bannister, The image theory quasi-static fields of antennas above the earth's surface, DTIC Document: 1969.

[5] P. R. Bannister and R. L. Dube, “Simple expressions for horizontal electric dipole quasi-static range subsurface-to-subsurface and subsurface-to-air propagation,” Radio Science, vol. 13, no. 3, pp. 501-507, 1978.

[6] P. R. Bannister, “Summary of image theory expressions for the quasi-static fields of antennas at or above the earth's surface,” Proceedings of the IEEE, vol. 67, no. 7, pp. 1001-1008, 1979.

[7] D. Chang and J. R. Wait, “Extremely low frequency (elf) propagation along a horizontal wire located above or buried in the earth,” IEEE Transactions on Communications, vol. 22, no. 4, pp. 421-427, 1974.

[8] R. W. King, “Electromagnetic field of a vertical dipole over an imperfectly conducting half-space, ” Radio Science, vol. 25, no. 2, pp. 149-160, 1990.

[9] R. W. King, C. W. Harrison and V. A. Houdzoumis, “Electromagnetic field in the sea due to an omnidirectional vlf antenna, ” Radio Science, vol. 32, no. 1, pp. 103-112, 1997.

[10] C. Tai and R. E. Collin, “Radiation of a hertzian dipole immersed in a dissipative medium,” IEEE Transactions on Antennas and Propagation, vol. 48, no. 10, pp. 1501-1506, 2000.

[11] R. Thottappillil, M. A. Uman and N. Theethayi, “Electric and magnetic fields from a semi-infinite antenna above a conducting plane,” Journal of Electrostatics, vol. 61, no. 3, pp. 209-221, 2004.

[12] P. K. Vong, D. Rodger and A. Marshall, “Modeling an electromagnetic telemetry system for signal transmission in oil fields,” IEEE Transactions on Magnetics, vol. 41, no. 5, pp. 2008-2011, 2005.

[13] X. B. Xu and Y. Huang, “An efficient analysis of vertical dipole antennas above a lossy half-space,” Progress In Electromagnetics Research, vol. 74, pp. 353-377, 2007.

[14] A. Khalatpour, R. Sarraf Shirazi and G. Moradi, “Analysis of vertical wire antennas above lossy half-space using matrix pencil method,” AEU-International Journal of Electronics and Communications, vol. 64, no. 8, pp. 784-789, 2010.

[15] M. Parise, “Second-order formulation for the quasi-static field from a vertical electric dipole on a lossy half-space,” Progress In Electromagnetics Research, vol. 136, pp. 509-521, 2013.

[16] J. R. Wait, “The electromagnetic fields of a horizontal dipole in the presence of a conducting half-space,” Canadian Journal of Physics, vol. 39, no. 7, pp. 1017-1028, 1961.

[17] V. Cooray, “Horizontal electric field above-and underground produced by lightning flashes,” IEEE Transactions on Electromagnetic Compatibility, vol. 52, no. 4, pp. 936-943, 2010.

[18] J. R. Wait and K. P. Spies, “On the image representation of the quasi-static fields of a line current source above the ground,” Canadian Journal of Physics, vol. 47, no. 23, pp. 2731-2733, 1969.

[19] O. Gavriloska, M. Mircev, V. Arnautovski and L. Grcev, “Approximate image formulation for the fields of a horizontal hertzian dipole in homogenous soil,” Proc. Int. PhD-Seminar Numerical Field Computation and Optimization in Electrical Engineering, 2005; pp 89-94.

[20] J. A. Stratton, Electromagnetic theory, John Wiley & Sons, 2007.

[21] R. F. Harrington and J. L. Harrington, Field computation by moment methods, Oxford University Press, 1996.